Spectral Analysis of Generic Rocket Wake Flows with Cold and Hot Exhaust Jets

By D. Kirchheck, D. Saile AND A. Gülhan

German Aerospace Center (DLR), Institute of Aerodynamics and Flow Technology
Supersonic and Hypersonic Technology Department
Linder Höhe, 51147 Cologne, Germany

The dynamic motions of the wake flow fields of a generic rocket launcher geometry at Mach 0.8, interacting with a supersonic exhaust jet at different stagnation conditions, ranging from 288 to 919 K are addressed in this work. They were analyzed regarding its spectral content by means of high-speed Schlieren imaging and unsteady chamber pressure measurements. The spectral analysis captured the typical wake flow frequencies and their characteristic mode shapes of the cross-flapping and swinging motions of the ambient shear layer at Sr_D = 0.19 and 0.35. At certain conditions, a strong amplification of the swinging motion was observed, which is probably governed by a coupling of the dynamic wake flow modes and the acoustic chamber properties.

1. Introduction

During the ascent, a rocket launcher is exposed to ever-changing environmental conditions. Correspondingly, the external flow constantly changes and so do loads imposed on the launch vehicle. This applies in particular to the afterbody of launch vehicles with a nozzle, subjected to the ambient flow [1]. The afterbody flow of a rocket launcher is similar to the flow around an axisymmetric *backward-facing step* (BFS). On average, the flow around a BFS forms a large scale annular recirculation region. That region is enclosed by the rocket's base surface, the nozzle surface and the shear layers between the recirculation, the cold ambient flow and the hot exhaust stream. Furthermore, the flow in the base region is highly unsteady. Instationary effects within the subsonic recirculation region act on the surface of the nozzle and base plate, but also impose effects farther downstream on the shear layer of the jet. Thus, the structures in the base region are exposed to local pressure fluctuations or periodic loads. Moreover, in some cases, there might be a coupling between the downstream and the upstream effects [2].

The reliable prediction of such highly transient load conditions is of great importance for the development of new components of future space transportation systems. For this reason, the subarea B of the *Collaborative Research Centre* (SFB) TRR40 is designated to investigate the base flow of rockets [3]. In that collaboration, experimental and numerical work is conducted in close cooperation between universities, public research institutions, and partners from the industry. The main objective of the collaboration is to provide flight-relevant data for a realistic modeling of the base flow effects. Over the past years, investigations by means of highly resolved flow simulations and wind tunnel experiments have been carried out by numerous different groups [3–12]. Within the SFB TRR40 (refer to Haidn et al. [3] for an overview on available literature), a wide Mach number range in the subsonic/transonic and supersonic/hypersonic regimes

($Ma_\infty = 0.5 \ldots 6.0$) has been investigated at free-stream Reynolds numbers of the order of 10^6 to 10^7 per meter. These parameters correspond to a typical trajectory of a launch system, such as the Ariane 5. Correspondingly, the geometric similarity is derived from that launcher. However, to capture the driving effects in a flight-realistic representation, more parameters have to be taken into account. Those are for example: the displacement effects of the rocket's exhaust jet, the temperature ratio between the external and internal flow, the shear layers of the detached base flow and the exhaust jet, and also the dynamic modes of the jet.

In previous experimental studies, the exhaust jet is modeled with a sting, formed according to the shape of the jet. Obviously, this approach only considers the displacement effects and it neglects the dynamics due to the flow interaction effects. Consequently, the jet is included by other groups. Its conditions are simulated by heating the gas to total temperatures of up to 600 K, and/or using helium instead of air [13]. Since helium features a comparable heat capacity ratio to the typical combustion products of *liquid oxygen and hydrogen* (LOX/LH2), vacuum exit velocities up to 2500 m/s are possible.

The goal of such an approach is to improve the similarity with the objective to gather more details on the imposing loads. The interaction of a cold ambient flow with a cold jet has been extensively investigated by Saile et al. [2, 14–16]. He finds a strong amplification of the base pressure and density gradient fluctuations for Mach 0.8 [2, 14]. This effect is associated with the extraordinary base flow dynamics in comparison to the other Mach number cases, which is described to be interrelated with the shedding of a vortex from the recirculation region [16]. Further, it is hypothesized that the strong amplification is the result of the resonating dynamics between the near-wake flow and the jet noise generation mechanism called screeching. In detail, evidence is found that the jet screech is in resonance with the swinging motion of the separated shear layer from the shoulder. In Saile's recent work [2], an attempt is made to transfer the findings above to the real flight and explain the significantly increased buffet loads of Ariane 5 in the subsonic flight regime. This was used as a starting point of the work at hand; however this time with a flight-realistic and hot exhaust jet in comparison to the cold jet. Investigations with a hot exhaust jet are practically non-existent since it requires actual hydrogen/oxygen combustion.

In the current report, wake flow phenomena of cold plume interaction and hot plume interaction test cases are compared, as well as the isolated ambient and exhaust flows. These were visualized by high-speed Schlieren imaging and post-processed using spectral decomposition methods of the two-dimensional density gradient fields. The results enable a comparison with previous findings in literature and lead the way for the design of future experiments in that field. The overarching goal hereby, was to further substantiate or clarify the hypothesis of jet screeching as being one of the driving mechanisms for rocket buffeting under dedicated flow conditions.

2. Experimental Setup and Methods

To investigate rocket base flow dynamics with regard to flow-flow-interaction between the ambient free stream and the propulsive jet, also referred to as the external and internal flows, the test object, an axisymmetric wind tunnel model, was located within the external wind tunnel flow. There it was supplied with the propulsive gas via its support structure. The internal flow was generated by expansion through the model's thrust nozzle at the base of the generic rocket.

2.1. *Hot Plume Testing Facility (HPTF)*

The test setup was located within the *Vertical Wind Tunnel Test Section (VMK)* of the *German Aerospace Center (DLR)* in Cologne. It included the necessary infrastructure to generate the external flow as well as the internal cold flow condition from a connected high-pressure air vessel. For the hot flow condition, the VMK is connected to a controlled *Gaseous Hydrogen and Oxygen (GH2/GO2) Supply Facility*, which feeds the model internal combustion chamber, where realistic stagnation conditions were generated prior to expanding the combustion gases through the models thrust nozzle. The VMK, its GH2/GO2 supply facility, the respective feed system for the wind tunnel model adapter, and the wind tunnel model itself comprise the *Hot Plume Testing Facility (HPTF)* of DLR (Figure 1), which is described in more detail in [17].

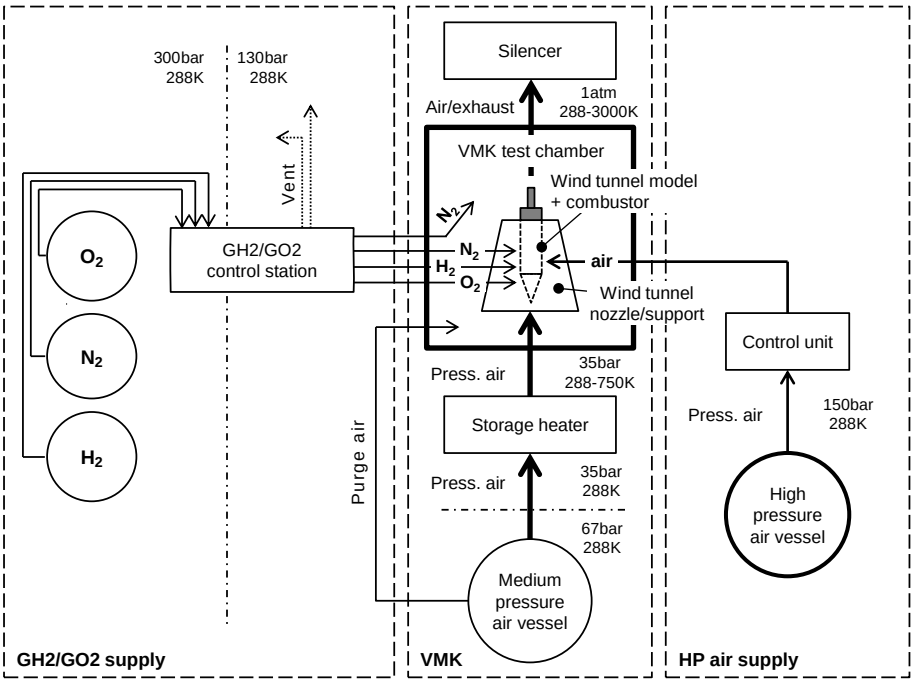

FIGURE 1. Schematic of the Hot Plume Testing Facility (HPTF), incorporating the Vertical Wind Tunnel Test Section (VMK), the GH2/GO2 supply facility, high-pressure air supply, and the test chamber, housing the wind tunnel nozzle and wind tunnel model, incl. the GH2/GO2 combustor

2.2. *Wind Tunnel Model*

The wind tunnel model is located on top of the central support structure, which is held within a cylindrical duct upstream of the convergent subsonic wind tunnel nozzle via eight tubes. They are used for supplying the model with combustion gases (2xGH2, 2xGO2) or high-pressure air, cabling for sensors and ignition, and optional coolant mass flow (Fig. 2). For both, the cold gas and hot gas tests, the thrust chamber geometry, including the nozzle contour were identical, except for the injection module. For the cold gas tests, the inner tube of the single element coaxial shear injector was removed to reach larger cross-sections with less pressure drop. A detailed description of the internal and external dimensions of the wind tunnel model can be found in [17] and [18].

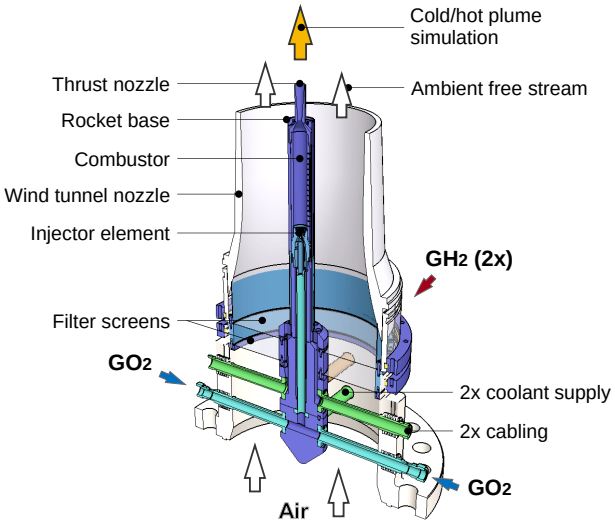

FIGURE 2. Wind tunnel nozzle with central upstream support, feed lines, and wind tunnel model extension

ID	Sensing task	Sensor type	x/mm	r/mm	ϕ/°	l_{trans}/mm
PS1	Steady pressure	Kulite XTEH-7L-190M-50BARA	0.00	16.00	-10	52.77
PI1	Unsteady pressure	Kulite XCE-062-30BARA	0.00	16.00	10	> 1000

TABLE 1. Combustion chamber instrumentation – sensor locations, type and nomenclature

2.3. *Instrumentation and Diagnostic Methods*

The characterization of the external flow was done by Pitot probe measurements with an additional static pressure port in the exit plane of the wind tunnel nozzle, approx. 11 mm upstream of the rocket base shoulder. The static pressure was used in a closed control loop for the setup of predefined ambient flow Mach numbers. The static free stream temperature for Mach number calculation was derived from isentropic relations, based on the total temperature inside the reservoir.

The combustor outflow properties were characterized by static and dynamic pressure measurements of the total chamber pressure. The chamber pressure was extracted from the base plate next to the injector outlet at the locations PI1 with a certain transmission length l_{trans} and PS1 as a static reference measurement without temperature influences at $l_{trans} > 1$ m. The unsteady pressure signals were analyzed regarding their spectral content to characterize the input conditions to the wake flow dynamics. All measurement data was acquired at 10 kHz. Fast Fourier Transformation (FFT) of the pressure signals were performed to obtain the power spectra S_{xx} for an evaluation time window of 2 s at 10 Hz frequency resolution. Further, a Hanning window with an overlap of 50% and arithmetic amplitude averaging was used. The controlled mass flows of oxygen and hydrogen were measured at the control station via Coriolis flow meters. The sensor locations in cylindrical coordinates with respect to the center of the chamber base plate is given in Tab. 1, together with their respective nomenclature.

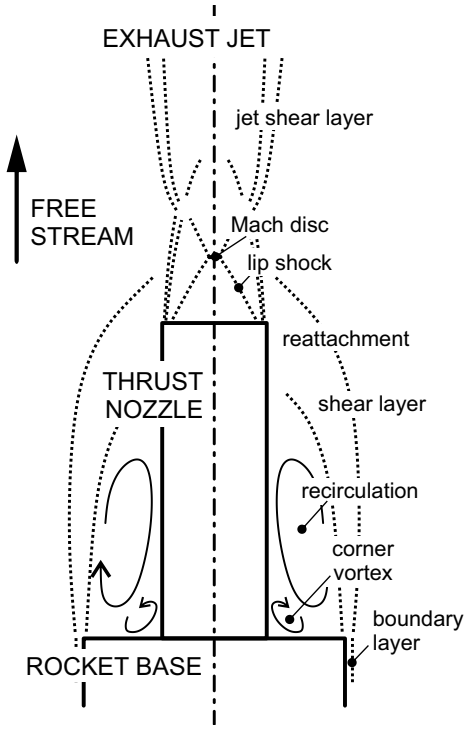

FIGURE 3. Typical topology of rocket base flow with an over-expanded exhaust jet and a thrust nozzle, exposed to the ambient reattaching shear layer

The present work shows our first approach of visualizing the flow topology for both, the cold plume and GH2/GO2 hot plume test cases in combination with ambient flow. For that, a Schlieren optics setup with high-speed imaging equipment within the topological region given in Fig. 3 was used. The recording frequency was 20 kHz with an exposure time of 2.5 µs. The goal was to analyze the Schlieren recordings with respect to their spectral content in order to identify and compare dominant frequencies, their intensities, and the local distribution in the wake between the different test cases. This was done by extracting the greyscale values of the images at specific image coordinates $I(x_{px}, y_{px})$ with I in $[0, 256]$ over time and performing an FFT of the time-resolved intensity fluctuations to obtain the power spectra. The FFT incorporated a 10 Hz frequency resolution with an overlap of 50 %. The investigated signal had a real time length of 0.5 s, consisting of 10,000 samples.

For a first global analysis, the amplitude spectra were spatially averaged within each frame, to easily identify the predominant frequencies. To further analyze the spatial distribution of the mean fluctuation amplitude and the dominant frequencies in the field, the results were plotted as spatial distribution at certain isolated frequencies in the image coordinate system by using band pass filtering with a filter width of 10 Hz.

2.4. *Test Matrix and Test Conditions*

The present work compares four main test cases at the critical ambient flow Mach number of 0.8 to investigate the main characteristics of the base flow dynamics and topolog-

ID	Jet flow	Ma_∞	p_∞ bar	T_∞ K	p_{cc} bar	T_{cc} K	a_{cc} m/s	$\dot{m}_{cc}$ g/s	OFR	u_e m/s
V087	Cold jet (only)	–	1.019	255.4*	19.17	288.0*	334.8*	459.9*	–	619.8*
V099	No jet	0.80	0.981	255.4*	–	–	–	–	–	
V098	Cold jet	0.80	0.987	255.4*	19.90	288.0*	334.8*	459.9*	–	619.8*
V097	Hot jet	0.80	0.992	255.4*	20.27	918.7*	1750.6*	89.40	0.693	2803.9*

* From one-dimensional analysis; $T_{amb} \approx 288\,K$

TABLE 2. Test matrix and test conditions

ical features with regard to the influence of a hot exhaust jet. First, the cold exhaust jet is measured without ambient flow (V087) and the wake flow is measured without an active exhaust jet (V099). The latter is broadly known in literature as an axisymmetric backward facing step flow and offers numerous validation sources. Then, a cold exhaust jet is added to this configuration (V098) which is then comparable to the preceding investigations of Saile et al. [2, 14]. Finally, the provided evaluation methods will be transferred to the case with a hot exhaust jet (V097). The first approach is to consequently keep the ambient flow and chamber conditions constant through all tests, as far as possible. The detailed test conditions are given in Tab. 2.

2.5. *Assessment of the Estimated Dominant Frequencies*

The findings from the spectral analysis were compared to typical dominant frequencies of specific types of flow features similar to, or included in, the flows under investigation, listed in Tab. 3. They were categorized in the acoustic and spatial modes of the model's pressure chamber, modes of the dynamic motion of the rocket wake flow, and acoustic phenomena from the jet dynamics. The characteristic frequencies of the pressure chamber and the jet dynamics vary with the jet temperature due to a changing sonic speed inside the chamber and a changing jet exit velocity [2, 14, 19]. However, for the wake flow dynamics, a temperature dependent model or similar measurements, showing possible

	Symbol	Cold jet	Hot jet	Unit	Reference
Model pressure chamber					
Helmholtz mode	f_{HH}	158.9	830.7	Hz	
First longitudinal mode	f_{1L}	656.5	3 432.5	Hz	[19]
Second longitudinal mode	f_{2L}	1 312.9	6 865.1	Hz	[19]
First tangential mode	f_{1T}	5 158.2	26 971.2	Hz	[19]
First radial mode	f_{1R}	10 720.6	56 056.0	Hz	[19]
Wake flow dynamics					
Cross-pumping motion	$f_{cp} = f\,(Sr_D = 0.1)$	376.5	376.5	Hz	[20]
Cross-flapping motion	$f_{cf} = f\,(Sr_D = 0.2)$	752.9	752.9	Hz	[20]
Swinging motion	$f_{sw} = f\,(Sr_D = 0.35)$	1 317.6	1 317.6	Hz	[20]
Jet dynamics					
Screeching	f_{sc}	1 246.9	1 329.7	Hz	[2, 14]

TABLE 3. Expected frequencies from external and internal flow dynamics and acoustics

influences from the jet temperature are not known by now. Therefore, as a first simplified assumption, the findings from [20] are applied to both, the cold and hot jet test cases. Detailed information on how the frequencies were estimated can be found in [17].

3. Experimental Results

In the following section, it is shown that in case of cold jet interaction, where the swinging motion matched the jet screeching frequency on the one hand and the 2L mode of the pressure chamber on the other hand, large fluctuations arose within the wake flow region. In contrast, this was not the case for the hot jet interaction experiments. Therefore, the analysis of the results focuses on the causalities and evaluates the different influences on the wake flow dynamics.

3.1. *Properties and Topological Features of the Mean Flow*

The data was analyzed for steady state input conditions. Reaching a steady state took the longest for the combustion chamber, which is shown in Fig. 4. The combustion chamber pressure was considered constant after 20s. Correspondingly, all mean flow quantities given in Tab. 2 refer to a common evaluation time window at $t_{\text{eval}} = [18.0\,, 20.0]\,\text{s}$, in which the flow conditions were maintained constant with acceptable deviations of the mean values.

The averaged Schlieren images (Fig. 5) give information about the mean flow topology. The density gradients show the shear layer evolving from the afterbody base plate. It allows a qualitative comparison of the reattachment length of the ambient shear layers. It seems that in relation to the ambient flow without jet (V099), the reattachment length is reduced in case of cold jet interaction (V098). In case of the hot jet interaction (V097), it is apparently the opposite. The reduction of the reattachment length for the cold jet (V098) is as expected due to turbulent entrainment of the jet. For the hot jet (V097), the contrary can be noted. Also note that Saile et al. [16] describe the reattachment location as being one possible driving parameter for the wake flow dynamics and that the excitation of the shear layer instabilities is largest when reattachment takes place at the nozzle tip.

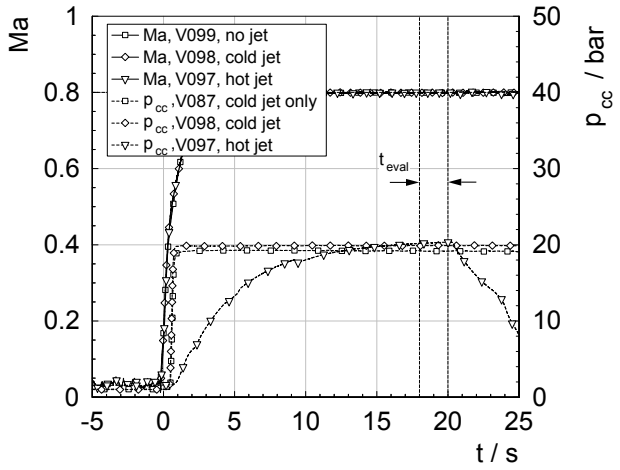

FIGURE 4. Major internal and external flow properties for all test cases in time; constant flow conditions are maintained within the evaluation time window at $t_{\text{eval}} = [18.0\,, 20.0]\,\text{s}$

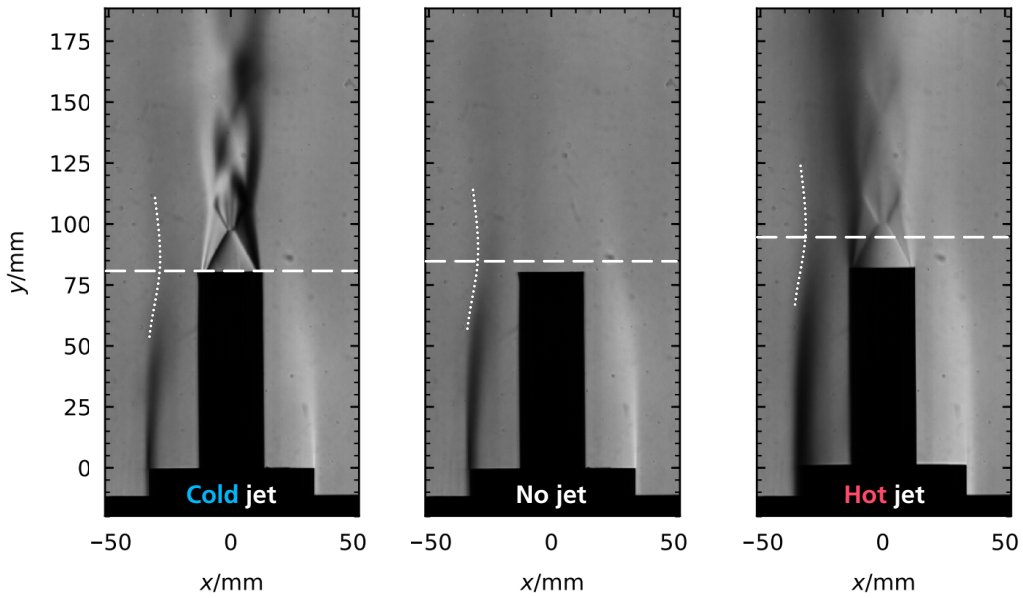

FIGURE 5. Averaged Schlieren images with qualitative comparison of the reattachment positions for ambient flows with (from left to right) cold jet (V098), no jet (V099), and hot jet (V097)

3.2. *Spectral Content of the Internal and External Flows*

The power spectra of the HSS intensity fluctuations are shown in Fig. 6(a)–6(c) for the ambient flow cases without jet, with cold jet, and with hot jet respectively. These were analyzed in combination with the power spectra of the dynamic total pressure measurements inside the model pressure chamber, which is shown in the following paragraphs.

The amplitude spectrum of the HSS images intensity fluctuations shows three major peaks (Fig. 6(a)). According to Tab. 3, the peaks at 700 Hz and around 1330 Hz can be assigned to the cross-flapping and swinging motion frequencies of the shear layer, estimated as f_{cf} = 753 Hz (Sr_D = 0.2) and f_{sw} = 1318 Hz (Sr_D = 0.35).

Next in Fig. 6(b), the chamber pressure spectra of the cold jet are discussed. At certain frequencies, the fluctuations are amplified in case of the interacting flow field, compared to the ambient flow without jet. In particular, this is true for the peaks at 1330 Hz and 1375 Hz, where the swinging motion is observed for the ambient flow without jet. In the preceding paragraph, the latter was assigned to the cross-flapping motion. Finally, the power spectrum is also increased at 1235 Hz, which is close to the estimated jet screeching frequency f_{sc} = 1247 Hz. The strong congruency of the chamber pressure spectrum and the estimated characteristic frequencies of the wake flow and jet dynamics yields to the hypothesis, that interaction, leading to an amplification of certain flow features might actually appear.

Investigating the HSS intensity spectrum of the cold jet interaction case (Fig. 6(b)), this hypothesis is emphasized by an extreme peak at around 1330 Hz, which again fits to the swinging motion frequency at f_{sw} = 1318 Hz as well as the 2L mode at f_{2L} = 1313 Hz. Further, these peaks appear up to its 4th harmonic frequency at 6640 Hz (only 1st and 2nd printed). This gives rise to the assumption that a strong coupling exists between the broadband chamber pressure oscillations around 1330 Hz, including the 2L mode and

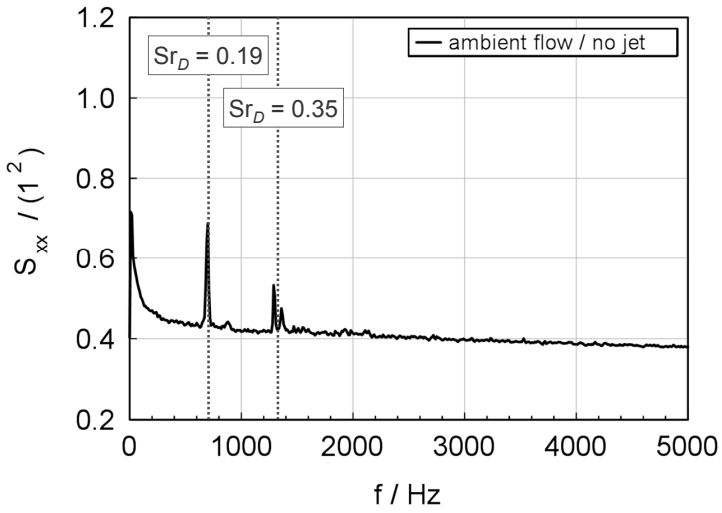

(a) Ambient flow without jet (V099)

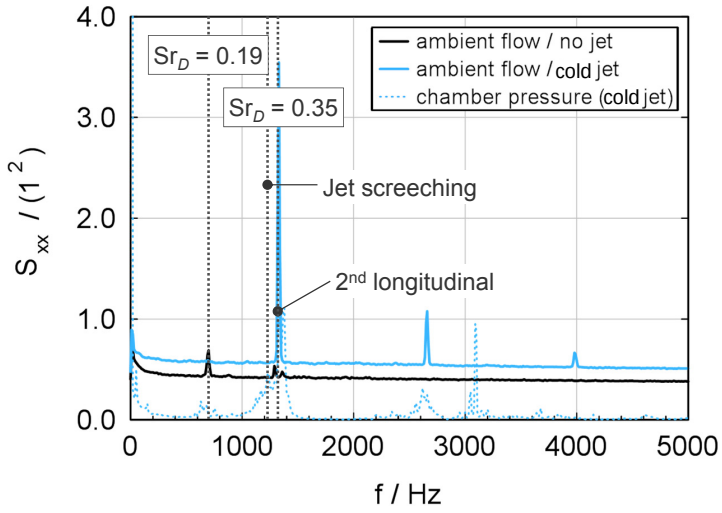

(b) Ambient flow with hot jet (V098)

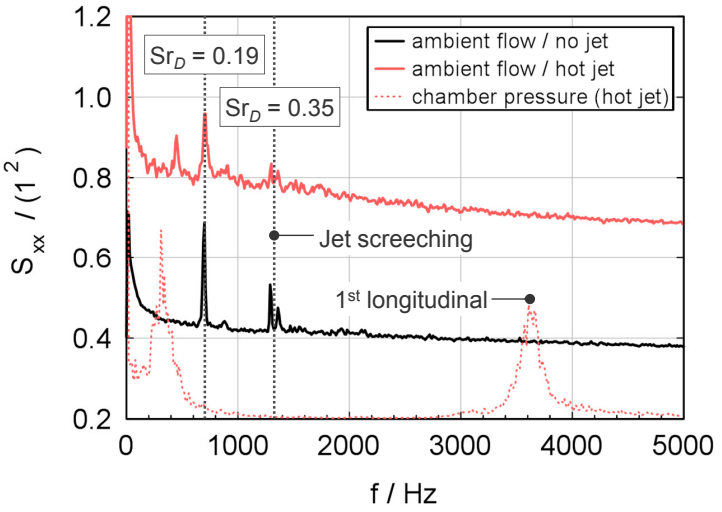

(c) Ambient flow with cold jet (V097)

FIGURE 6. HSS power spectra of ambient flow cases without jet (V099), with cold jet (V098), and with hot jet (V097); comparison with chamber pressure spectra and estimated screeching frequencies

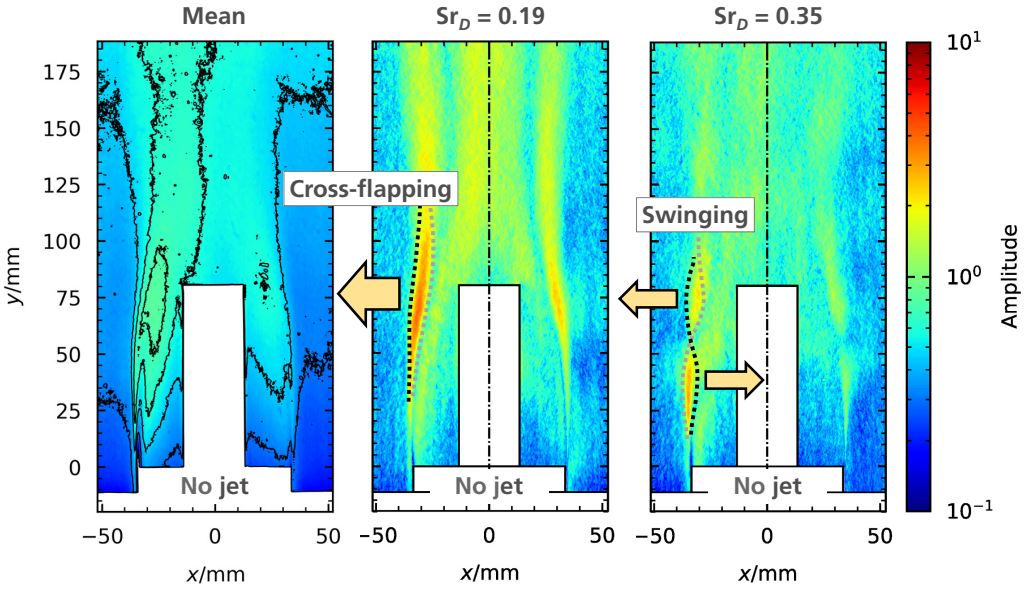

FIGURE 7. Amplitude distribution of the power spectrum for ambient flow without jet (V099); left - mean amplitude distribution; middle - amplitude distribution for $Sr_D = 0.19$ (cross-flapping motion); right - amplitude distribution for $Sr_D = 0.35$ (swinging motion)

the screeching frequency, and the swinging motion of the shear layer. What is unclear at this point is to which extent the three different frequencies contribute to the observed amplification.

The power spectrum of the HSS intensity fluctuations from the hot jet case (Fig. 6(c)) shows a slightly higher mean level compared to the cold jet case. However, the amplitude level is highly depending on the optical setup and the dynamic range of the global density. Since the hot jet density is significantly deviating from the cold jet density by approximately one order of magnitude, this effect might be related to the generally higher density gradients in the field. Further, the spectrum does not reveal increased peaks referred to chamber oscillations. This means that no distinct excitation of the near-wake flow takes place due to fluctuations in the chamber. Nevertheless, peaks can be detected at the same characteristic frequencies as found for the ambient flow without jet (700 Hz, 1290 Hz, and 1360 Hz). Therefore, the flow field is dominated by the well-known near-wake flow dynamics such as the cross-flapping and swinging motion. However, the previously found strong excitation mechanisms and presumable coupling phenomena cannot be detected in this case.

3.3. *Spatial Distribution of the Dominant Isolated Frequencies*

In Section 3.2, various spectral features of the chamber pressure and HSS intensity fluctuations for the different configurations are assigned to the characteristic wake flow modes, as determined in Section 2.5. Although, the agreement with the prediction is remarkable for some frequencies, deviations occur. Thus, final statements can neither be given solely by the assessment of the power spectra, nor the field averaged intensity fluctuations from HSS images, since only the temporal characteristics of the flow field are characterized so far. To finally evaluate the distinctive features of the spectra, they should also be linked to a spatial characteristic, or eigenmode, of the flow field's motion.

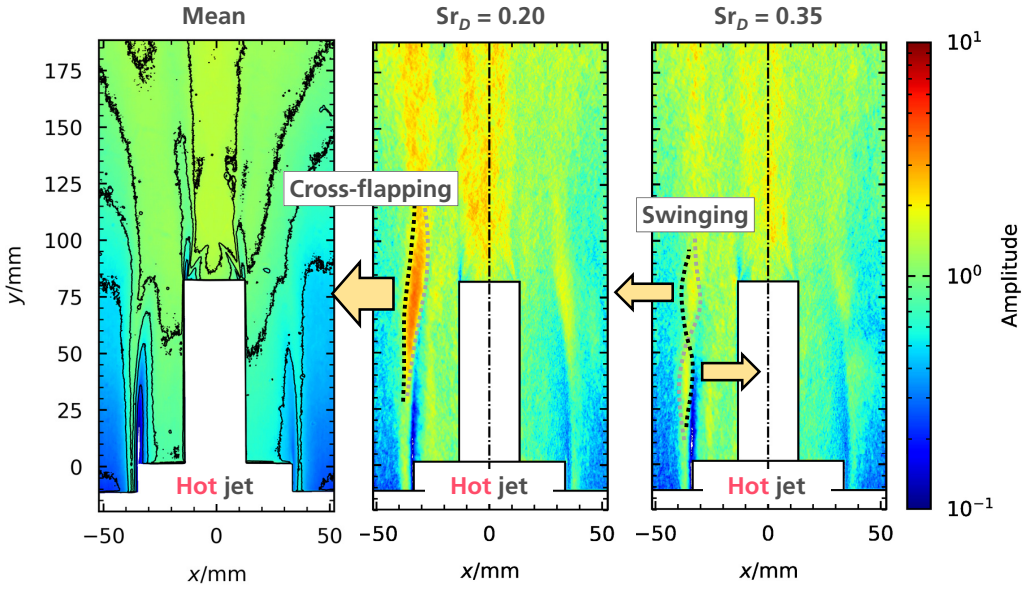

FIGURE 8. Amplitude distribution of the power spectrum for ambient flow with hot jet (V097); left - mean amplitude distribution; middle - amplitude distribution for Sr_D = 0.2 (cross-flapping motion); right - amplitude distribution for Sr_D = 0.35 (swinging motion)

This is done in the following section by analyzing the spatial distribution of the amplitude of isolated frequencies in the wake flow field, according to Section 2.3.

For the ambient flow without jet, the two most dominant frequencies, 700 Hz and 1290 Hz, corresponding to the non-dimensional frequencies of Sr_D = 0.19 and Sr_D = 0.34, respectively, are plotted in Fig. 7 as two-dimensional fields of the power spectrum amplitude, next to the mean fluctuation amplitude. They correspond to the peaks found in the spatial average of the power spectra (Fig. 6(a)). In both cases, it is obvious, that the higher amplitudes, which lead to the peak in the average power spectrum are located in the ambient shear layer as well as the wake of the nozzle in which the circular shear layer can interact with itself. Further, for the 700 Hz, the peak amplitudes are found near the nozzle tip in a slim axially elongated region, which is an indication for lateral fluctuations at that place. The same is true for the 1290 Hz distribution, except that the peak region is now split in two sections, which, assuming a 180° phase shift between the two sections would result in a swinging motion in the cross direction. Comparing these topologies with the results of the modal decomposition by Statnikov et al. [20] and Saile [2], the evidence is that the identified spectra at 700 Hz and 1290 Hz can indeed be characterized as the cross-flapping motion and swinging-motion of the shear layer.

As expected from the average HSS power spectra, the ambient flow case with hot jet interaction behaves similarly to the ambient flow without jet regarding the frequencies of the cross-flapping and swinging motion. In Fig. 8, they are plotted in their most intensified bands, which are 710 Hz for the cross-flapping motion (middle) and 1300 Hz for the swinging motion (right), which corresponds to Sr_D = 0.2 and Sr_D = 0.35. Compared to the ambient flow without jet, the mean amplitude is increased in the whole interacting flow regime. In particular, this is true inside the jet and in the far wake of the bluff body, where the shear layers are interacting strongly, but also the recirculation itself experiences larger fluctuations. Note that the Schlieren technique is an integrating method

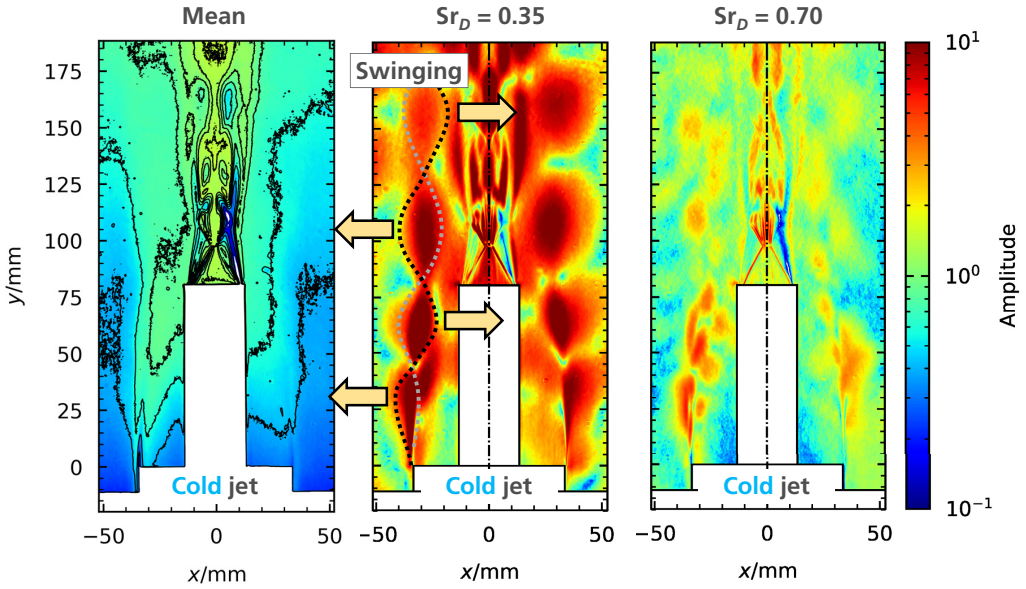

FIGURE 9. Amplitude distribution of the power spectrum for ambient flow with cold jet (V098); left - mean amplitude distribution; middle - amplitude distribution for $Sr_D = 0.35$ (swinging motion); right - amplitude distribution for $Sr_D = 0.7$ (swinging motion 1st harmonic)

and that fluctuations from the shear layers parallel to the coordinate plane inevitably contribute to the illustrated quantities.

The two most intensified frequencies (1330 Hz and 2660 Hz, corresponding to Sr_D = 0.35 and Sr_D = 0.7) from the HSS power spectrum for the ambient flow case with cold jet interaction are plotted in Fig. 9. From the preceding results, they were described as a coupling of the swinging-motion frequency with the first and second longitudinal mode of the pressure chamber and optionally the screeching frequency. It can be seen that for Sr_D = 0.35 the extreme peak in the average HSS spectrum indeed comes from a zonal increase of the fluctuation amplitude, rather than a global homogeneous increase of the mean fluctuation. Most of the fluctuation energy is concentrated in circular structures, emanating from the base shoulder and continuing within the shear layer into the far wake. The dimension of those clusters of increased amplitude is growing in the stream-wise direction and their location seems to be about symmetrical along the center axis. Interpreting the findings under the assumption of a generally lateral cross movement of the density gradient field at the location of those clusters, the locations between the clusters with negligible amplitude are identified as stationary nodes of a swinging motion of the shear layer. Note that this excitation was already elaborated in Saile [2, 14–16] by means of PIV and pressure measurements. There it is seen as aeroacoustic coupling mechanism between the swinging motion and jet screeching.

Next to the swinging motion of the shear layer, an increase of fluctuation amplitudes is also visible within the jet shear layer, with a significant extent developing downstream of the first Mach disc. Although not fully visible, the structure, which is similarly elongated in the stream-wise direction within the jet shear layer, seems to be repeating at y = 175 mm and showing the same characteristics as the ambient shear layer. The origin of this phenomenon is seen in the wake flow, imposing a periodically fluctuating pressure field on the supersonic jet, which itself is consequently subjected to a swinging motion. While

the first shock cell is still quite stable, the swinging motion is potentially increasing in the stream-wise direction since both, the effect of the wake flow field as well as the intrinsic disturbances within the jet shear layer should grow while propagating downstream.

Finally, the amplitude distribution of $Sr_D = 0.7$, still shows the clustered structure in the ambient shear layer, while the dimension of each cluster is reduced by about half for each of the higher harmonics. This is also an indicator for a truly periodic movement at 1330 Hz, although, the higher harmonics are less prominent in the wake and in the jet.

4. Conclusion and Outlook

Spectral analyzes of the wake flow of a generic rocket launcher geometry at flow Mach number 0.8, interacting with a supersonic exhaust jet by means of HSS imaging revealed large differences in the fluctuating density gradient field between flow configurations with cold or hot exhaust jet. The hot exhaust jet was generated by means of GH2/GO2 combustion inside the wind tunnel model combustion chamber, which is rather unique for base flow investigations. Analytical estimations of the acoustic properties of the pressure chamber, the characteristic wake flow modes, and the dynamic features of the supersonic jet were compared with spectral analyzes of the HSS intensity fluctuations of the near-wake and the total chamber pressure measurements. The objective was to evaluate the remarkable features of the near-wake dynamics with respect to their driving mechanisms.

The cases of ambient flow without jet and ambient flow with hot jet showed the typical wake flow modes, which were in good agreement with the estimated non-dimensional frequencies from literature, such as Statnikov et al. [20]. The same appeared to be true for the distribution of density gradient fluctuations, which were very similar to the results of Statnikov et al. [20] with respect to the form and location of the excited areas. The cross-flapping motion was measured at 700 Hz/710 Hz ($Sr_D = 0.19$) for the cases without jet and with hot jet respectively. The swinging motion was detected in the range of 1290 Hz ($Sr_D = 0.34$) and 1360Hz ($Sr_D = 0.36$). The chamber pressure measurements of ambient flow without jet showed peaks in the same regions with a slight frequency shift (760 Hz for the cross-flapping motion), which qualitatively validates the HSS analysis. Additional pressure measurements in the base could enable a final quantitative characterization in future tests.

The ambient flow case with cold exhaust jet showed a resonance peak at 1330 Hz ($Sr_D = 0.35$) in the spatially averaged spectrum of the HSS intensity fluctuations. The resonance frequency corresponds both, to the estimated swinging motion frequency of the ambient shear layer and the second longitudinal mode (2L) of the pressure chamber, which was also identified in the chamber pressure measurements. The characteristics of the swinging motion were identified by the shape and location of the spatially distributed amplitude of its isolated frequency. Its amplification appears to be more emphasized for the cold than for the hot jet case. However, it must be kept in mind that the scale of the density gradient is strongly dependent on the setting. Associating a quantitative meaning (except for the frequency) is difficult. Finally, it is assumed that a strong coupling exists between the swinging motion of the ambient shear layer and the fluctuating jet shear layer due to the measured chamber pressure fluctuations at its second longitudinal mode.

This deviates from the hypothesis in Saile [2]. There, the same extraordinary excitation is found in the near-wake for a configuration with cold jet and an ambient flow at

Mach 0.8 However, it is suggested that jet screech instead of chamber instabilities is the driving mechanism for the amplification of the wake flow modes. For the present study, the estimated screeching frequencies for the cold and hot jet cases (1247 Hz/1330 Hz) were lying close to the amplified band of the HSS fluctuations and, consequently, to the swinging motion frequency of the ambient shear layer. But, since it was not isolated from the acoustic modes of the pressure chamber for the cold jet case, it is still unclear, which contribution it makes to the observed amplification. Here, the data from the hot jet tests could be consulted for clarification. In this configuration, no such strong amplification of the swinging motion existed, although, the swinging motion and jet screeching frequencies matched perfectly.

Another explanation might be, that the reattachment of the ambient shear layer is not clearly defined for the hot jet case. Saile et al. [2, 16] finds a strong dependency between the shear layer reattachment location and the excitation of the near-wake flow. For the case at hand, the averaged Schlieren images indicated a reattachment farther downstream on the jet, but not on the solid nozzle wall. This might cause a dampening of the vortex shedding mechanism and its corresponding excitation as seen in Saile et al. [2, 16].

Unfortunately, the Schlieren recordings could not capture the reattachment location precisely. Consequently, further studies are suggested to evaluate the reattachment length and to address the sensitivity of the observed excitation with respect to the reattachment of the ambient shear layer. This could be done by modifying the length of the thrust nozzle. Further, to separate the various influences, it is suggested to shift the chamber frequency to a different frequency range, e. g. by modifying the internal chamber geometry. Thus, the different contributions, either of the acoustic chamber modes or the dynamics of the supersonic jet to the excitation of the wake flow modes, could be considered separately.

Acknowledgments

Financial support has been provided by the German Research Foundation (Deutsche Forschungsgemeinschaft – DFG) in the framework of the Sonderforschungsbereich Transregio 40. The support of the technical staff during the work at the Supersonic and Hypersonic Technologies Department in Cologne is highly appreciated.

References

[1] DAVID, S. AND RADULOVIC, S. (2005). Prediction of Buffet Loads on the Ariane 5 Afterbody. In: *6th International Symposium on Launcher Technologies*. Munich, Germany.

[2] SAILE, D. *Experimental Analysis on Near-Wake Flows of Space Transportation Systems*. Ph.D. thesis, Rheinisch-Westfälische Technische Hochschule (RWTH) Aachen. Submitted in February 2019.

[3] HAIDN, O.J., ADAMS, N.A., SATTELMLAYER, T., STEMMER, C., RADESPIEL, R., SCHRÖDER, W. AND WEIGAND, B. (2018). Fundamental Technologies for the Development of Future Space Transportsystem Components under high Thermal and Mechanical Loads. In: *2018 Joint Propulsion Conference*. 9–11 July, Cincinnati, Ohio. AIAA 2018-4466.

[4] SCHOONES, M. AND BANNINK, W. (1998). *Base flow and exhaust plume interaction. Part 1: Experimental study*. Delft University Press. ISBN 9040717478.

[5] SCHOONES, M. AND HOUTMAN, E. (1998). *Base flow and exhaust plume interaction. Part 2: Computational study*. Delft University Press. ISBN 9040717486.

[6] DEPRÉS, D., REIJASSE, P. AND DUSSAUGE, J.P. (2004). Analysis of Unsteadiness in Afterbody Transonic Flows. *AIAA Journal*, **42**(12), 2541–2550.

[7] DECK, S. AND THORIGNY, P. (2007). Unsteadiness of an Axisymmetric Separating-Reattaching Flow: Numerical Investigation. *Physics of Fluids*, **19**(065103), 1–20.

[8] ÉLIE WEISS, P., DECK, S., ROBINET, J.C. AND SAGAUT, P. (2009). On the Dynamics of Axisymmetric Turbulent Separating/Reattaching Flows. *Physics of Fluids*, **21**(7), 1–8.

[9] HANNEMANN, K., LÜDECKE, H., PALLEGOIX, J.F., OLLIVIER, A., LAMBARÉ, H., MASELAND, H., GEURTS, E., FREY, M., DECK, S., SCHRIJER, F., SCARANO, F. AND SCHWANE, R. (2011). Launch Vehicle Base Buffeting-Recent Experimental and Numerical Investigations. In: *7th European Symposium on Aerothermodynamics*. 9–12 May, Brugge, Belgium.

[10] SCHRIJER, F., SCIACCHITANO, A. AND SCARANO, F. (2014). Spatio-Temporal and Modal Analysis of Unsteady Fluctuations in a High-subsonic Base Flow. *Physics of Fluids*, **26**(8), 86–101.

[11] SCHWANE, R. (2015). Numerical Prediction and Experimental Validation of Unsteady Loads on ARIANE5 and VEGA. *Journal of Spacecraft and Rockets*, **52**(1).

[12] VAN GENT, P., PAYANDA, Q., BRUST, S., VAN OUDHEUSDEN, B.W. AND SCHRIJER, F. (2017). Experimental Study of the Effects of Exhaust Plume and Nozzle Length on Transonic and Supersonic Axisymmetric Base Flows. In: *7th European Conference for Aeronautics and Space Sciences (EUCASS)*. 3–6 July, Milan, Italy.

[13] STEPHAN, S. AND RADESPIEL, R. (2017). Propulsive Jet Simulation with Air and Helium in Launcher Wake Flows. *CEAS Space Journal*, **9**(2), 195–209.

[14] SAILE, D., KÜHL, V. AND GÜLHAN, A. (2019). On the subsonic near-wake of a space launcher configuration without jet. *Experiments in Fluids*, **60**(4), 50. ISSN 1432-1114. DOI 10.1007/s00348-019-2690-9. URL `https://doi.org/10.1007/s00348-019-2690-9`.

[15] SAILE, D., KÜHL, V. AND GÜLHAN, A. On the subsonic near-wake of a space launcher configuration with jet. *Experiments in Fluids*. Submitted and considered for publication after revision in April 2019.

[16] SAILE, D., KÜHL, V. AND GÜLHAN, A. (2019). On Subsonic Near-Wake Flows of Various Base Geometries. In: *13th International Symposium on Particle Image Velocimetry (ISPIV)*. 22–24 July, Munich, Germany.

[17] KIRCHHECK, D., SAILE, D. AND GÜLHAN, A. (2019). Spectral Analysis of Rocket Wake Flow-Jet Interaction by Means of High-speed Schlieren Imaging. In: *8th European Conference for Aeronautics andSpace Sciences (EUCASS)*. 1–4 July, Madrid, Spain.

[18] KIRCHHECK, D. AND GÜLHAN, A. (2017). Interaktionsteststand für realistische Raketentreibstrahlen mit umströmender Atmosphäre. In: *Deutscher Luft- und Raumfahrtkongress 2017*. 5–7 September, Munich, Germany.

[19] BLOMSHIELD, F.S. (2007). Lessons Learned In Solid Rocket Combustion Instability. In: *43rd AIAA/ASME/SAE/ASEE Joint Propulsion Conference & Exhibit*. 8–11 July, Cincinnati, Ohio.

[20] STATNIKOV, V., MEINKE, M. AND SCHRÖDER, W. (2017). Reduced-order analysis of buffet flow of space launchers. *Journal of Fluid Mechanics*, **815**, 1–25.